Understanding Ultrasonic Ranging Sensors

How the popular Polaroid sonar unit works and considerations for use on mobile robots for obstacle avoidance and navigation.

by H.R. Everett
Adapted from the book Sensors for Mobile Robots: Theory and Application, *published by AK Peters, Ltd, Wellesley, MA*
ISBN 1-56881-048-2

The Polaroid ranging module is an active time of flight (TOF) device developed for automatic camera focusing. It determines the range to target by measuring elapsed time between transmission of an ultrasonic waveform and the detected echo (Biber, et al., 1980). Probably the single most significant sensor development from the standpoint of its catalytic influence on the robotics research community, this system is widely found in the literature (Koenigsburg, 1982; Moravec & Elfes, 1985; Everett, 1985; Kim, 1986; Arkin, 1989; Borenstein & Koren, 1990). Representative of the general characteristics of a number of such ranging devices, the Polaroid unit soared in popularity as a direct consequence of its extremely low cost (the transducer and ranging module circuit board are available for less than $50), made possible by high-volume usage in its original application as a camera autofocus sensor.

Introduction to Sonar Sensors

All sensors, whether active or passive, perform their function by detecting (and in most cases quantifying) the change in some specific property (or properties) of energy. Active sensors emit energy that travels away from the sensor and interacts with the object of interest, after which part of the energy is returned to the sensor. For passive sensors, the source of the monitored energy is the object itself and/or the surrounding environment. In the case of acoustical systems, it must be recognized that the medium of propagation can sometimes have significant influence, and such effects must be taken into account.

Sound is a vibratory mechanical perturbation that travels through an elastic medium as a longitudinal wave. For gases and liquids the velocity of wave propagation is given by (Pallas-Areny & Webster, 1992):

$$s = \sqrt{\frac{K_m}{\rho}}$$

where:
s = speed of propagation
K_m = bulk modulus of elasticity
ρ = density of medium.

Since the introduction of sonar in 1918, acoustic waves have been successfully used to determine the position, velocity, and orientation of underwater objects in both commercial and military applications (Ulrich, 1983). It therefore seems only logical we should be able to take advantage of this well-developed technology for deployment on mobile robotic vehicles. This seemingly natural carryover from underwater scenarios has been somewhat lacking, however, for a number of reasons. The speed of sound in air (assume sea level and 25°C) is 1138 feet/second, while under the same conditions in seawater sound travels 5,034 feet/second (Bolz & Tuve, 1979). The wavelength of acoustical energy is directly proportional to the speed of propagation as shown below:

$$\lambda = \frac{s}{f}$$

where:
λ = wavelength
s = speed of sound
f = operating frequency.

This relationship means the wavelength for an underwater sonar operating at 200 KHz would be approximately 0.30 inches, while that associated with operation in air at the same frequency is in contrast only 0.07 inches. As we shall see later, the shorter the wavelength, the higher the achievable resolution. So in theory, better resolution should be obtainable with sonar in air than that associated with operation in water. In practice, however, the performance of sonar operating in air seems poor indeed in comparison to the success of underwater implementations, for several reasons.

For starters, water (being basically incompressible) is a much better conductive medium (for sound) than is air. In fact, sound waves originating from sources thousands of miles away are routinely detected in oceanography and military applications. One such example involves monitoring global warming (as manifested in long-term variations in average sea-water temperature) by measuring the associated change in the speed of wave propagation over a transoceanic path.

Secondly, the mismatch in acoustical impedance between the transducer and the conducting medium is much larger for air than water, resulting in reduced coupling efficiency. The high acoustic impedance of water allows for conversion efficiencies from 50 to 80 percent, depending on the desired bandwidth (Bartram, et al., 1989). In addition, underwater systems are generally looking for fairly large discrete targets in relatively non-interfering surroundings, with the added benefit of intensely powerful pulse emissions.

And finally, one should keep in mind that untold billions of defense dollars have been invested over many decades in the research and development of sophisticated underwater systems that individually cost millions of dollars to procure, operate, and maintain. In contrast, most robotic designers begin to balk when the price of any sensor subsystem begins to exceed a few thousand dollars.

The range of frequencies generally associated with human hearing runs from about 20 Hz to somewhere around 20 KHz. Although sonar systems have been developed that operate (in air) within this audible range, ultrasonic frequencies (typically between 20 KHz and 200 KHz) are by far the most widely applied. It is interesting to note, however, ultrasonic frequencies as high as 600 MHz can be produced using piezoelectric quartz crystals, with an associated wavelength in air of 500 nanometers (Halliday & Resnick, 1974). (This wavelength is comparable to electromagnetic propagation in the visible light region of the energy spectrum.) Certain piezoelectric films can be made to vibrate in the gigahertz range (Campbell, 1986).

Acoustical ranging can be implemented using triangulation, time of flight (Frederiksen & Howard, 1974; Biber, et al., 1980), frequency modulation (Mitome, et al., 1984), phase-shift measurement (Fox, et al., 1983; Figueroa & Barbieri, 1991), or some combination of these techniques (Figueroa & Lamancusa, 1992). Triangulation and time-of-flight methods typically transmit discrete short-duration pulses and are effective for in-close collision avoidance needs, and at longer distances for navigational referencing. Frequency-modulation and phase-shift ranging techniques involving the transmission of a continuous sound wave are better suited for short-range situations where a single dominant target is present.

Ultrasonic-based measurement systems have found broad appeal throughout the industrial community for a wide variety of purposes such as non-destructive testing (Campbell, 1986), industrial process control (Asher, 1983), stock measurement (Shirley, 1991), liquid level measurement (Shirley, 1989), safety interlocks around dangerous machinery (Irwin & Caughman, 1985), and even intrusion detection in security scenarios (Smurlo & Everett, 1993). In the recreational electronics industry, major usage is seen in underwater sonar for depth and fish finding (Frederikson & Howard, 1974), and automatic camera focusing (Biber, et al., 1980). Typical robotic applications include collision avoidance (Everett, 1985), position location (Dunkin, 1985; Figueroa & Mahajan, 1994), and Doppler velocity measurements (Milner, 1990).

Figure 1: *ROBART II, an autonomous security robotic testbed, employs a total of 36 Polaroid electrostatic transducers for collision avoidance, navigational referencing, and intrusion detection.*

Polaroid Ultrasonic Ranging Module

The most basic configuration of the Polaroid ranging module consists of two fundamental components: 1) the ultrasonic transducer and 2) the ranging module electronics. A choice of transducer types is now available. In the original instrument-grade electrostatic version, a very thin metalized diaphragm mounted on a machined backplate forms a capacitive transducer (Polaroid, 1981). A smaller electrostatic transducer (7000-Series) has also been made available, developed for the Polaroid Spectra camera (Polaroid, 1987). A ruggedized piezoelectric (9000-Series) environmental transducer introduced for applications that may be exposed to rain, heat, cold, salt spray, and vibration is able to meet or exceed guidelines set forth in SAE J1455 January 1988 specification for heavy-duty trucks.

The original Polaroid ranging module (607089) functioned by transmitting a chirp of four discrete frequencies in the neighborhood of 50 KHz. The SN28827 module was later developed with a reduced parts count, lower power consumption, and simplified computer interface requirements. This second-generation board transmits only a single frequency at 49.1 KHz. A third-generation board (6500 series) introduced in 1990 provided yet a further reduction in interface circuitry, with the ability to detect and report multiple echoes (Polaroid, 1990). An Ultrasonic Ranging Developer's Kit based on the Intel 80C196 microprocessor is now available that allows software control of transmit frequency, pulse width, blanking time, amplifier gain, and achieved range measurements from 1 inch to 50 feet (Polaroid, 1993).

The ultrasonic ranging capability of ROBART II (Figure 1) is based entirely on the Polaroid system (three SN28827 ranging modules each multiplexed to 12 electrostatic transducers). For obstacle avoidance purposes, a fixed array of 11 transducers is installed on the front of the body trunk (as shown in the photo) to provide distance information to objects in the path of the robot. A ring of 24 additional ranging sensors (15 degrees apart) is mounted just below the robot's head and used to gather range information for position estimation. A final ranging unit is located on the rotating head assembly, allowing for distance measurements to be made in various directions. Reliability of the Polaroid components has been exceptional, with no failures or degraded performance of any type in over eight years of extended operation.

A typical operating cycle is as follows:

- The control circuitry fires the transducer and waits for an indication that transmission has begun.
- The receiver is blanked for a short period of time to prevent false detection due to residual transmit signal ringing in the transducer.
- The received signals are amplified with increased gain over time to compensate for the decrease in sound intensity with distance.
- Returning echoes that exceed a fixed-threshold value are recorded and the associated distances calculated from elapsed time.

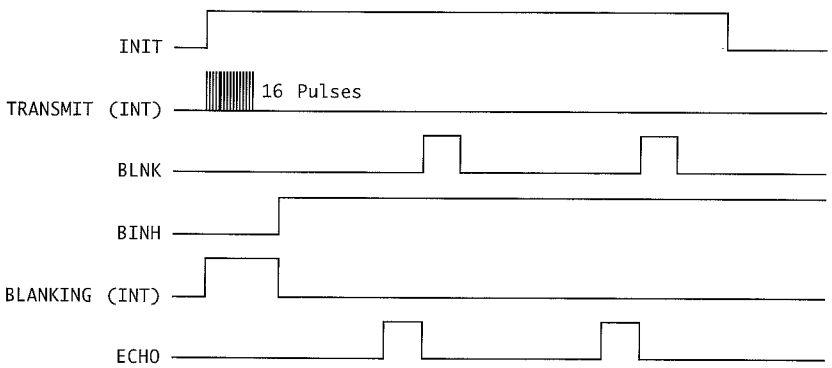

Figure 2: *Timing diagrams for the 6500-Series Sonar Ranging Module executing a multiple-echo-mode cycle with blanking input (courtesy Polaroid Corp).*

In the single-echo mode of operation for the 6500-series module, the blank (BLNK) and blank-inhibit (BINH) lines are held low as the initiate (INIT) line goes high to trigger the outgoing pulse train. The internal blanking (BLANKING) signal automatically goes high for 2.38 milliseconds to prevent transducer ringing from being misinterpreted as a returned echo. Once a valid return is received, the echo (ECHO) output will latch high until reset by a high-to-low transition on INIT. For multiple-echo processing, the blank (BLNK) input must be toggled high for at least 0.44 milliseconds after detection of the first return signal to reset the echo output for the next return as shown in Figure 2 (Polaroid, 1990).

Performance Factors

There are three basic types of ultrasonic transducers: 1) magnetostrictive, 2) piezoelectric, and 3) electrostatic. The first of these categories, magnetostrictive, is primarily used in high-power sonar and ultrasonic cleaning applications (Campbell, 1986), and is of limited utility from a mobile robotics perspective. Piezoelectric transducers (sometimes referred to as piezoceramic) are electrically similar to quartz crystals and resonant at only two frequencies: the resonant and antiresonant frequencies (Pletta, et al., 1992). Transmission is most efficient at the resonant frequency while optimum receiving sensitivity occurs at the antiresonant frequency (National, 1989). In bistatic (dual transducer) systems, the resonant frequency of the transmitting transducer is matched to the antiresonant frequency of the receiver for optimal performance.

Piezoelectric crystals change dimension under the influence of an external electrical potential and will begin to vibrate if the applied potential is made to oscillate at the crystal's resonant frequency. While the force generated can be significant, the displacement of the oscillations is typically very small, and so piezoelectric transducers tend to couple well to solids and liquids but rather poorly to low-density compressible

media such as air (Campbell, 1986). Fox, et al. (1983) report using a quarter-wavelength silicon-rubber matching layer on the front face of the transducer in an attempt to achieve better coupling into air at operating frequencies of 1 to 2 MHz. There is also a mechanical inertia associated with the vibrating piezoelectric crystal. As a consequence, such transducers will display some latency (typically several cycles) in reaching full power, and tend to "ring down" longer as well when the excitation voltage is removed.

Electrostatic transducers, on the other hand, generate small forces but have a fairly large displacement amplitude, and therefore couple more efficiently to a compressible medium such as air than do piezoelectric devices. The low-inertia foil membrane allows for quicker turn-on and turn-off in comparison to the slow response of piezoelectrics, facilitating unambiguous short-duration pulses for improved timing accuracy (Campbell, 1986). Since effective operation is not limited to a unique resonance frequency, electrostatic transducers are much more broadband, but with an upper limit of several hundred kilohertz in contrast to megahertz for the piezoelectric variety.

In addition to transducer design considerations, the performance of ultrasonic ranging systems is significantly affected by target characteristics (i.e., absorption, reflectivity, directivity) and environmental phenomena, as will be discussed below.

Atmospheric Attenuation. As an acoustical wave travels away from its source, the signal power decreases according to the inverse square law as illustrated in Figure 3, dropping 6 dB as the distance from the source is doubled (Ma & Ma, 1984). The following describes the effects of spherical divergence on signal intensity:

$$I = \frac{I_o}{4\pi R^2}$$

where:
I = intensity (power per unit area) at distance R
I_o = maximum (initial) intensity
R = range.

There is also an exponential loss associated with molecular absorption of sound energy by the medium itself (Pallas-Areny & Webster, 1992):

$$I = I_o\, e^{-2\alpha R}$$

where:
α = attenuation coefficient for medium.

The value of α varies slightly with the humidity and dust content of the air and is a function of the operating frequency as well (i.e., higher frequency transmissions attenuate at a faster rate). The maximum detection range for an ultrasonic sensor is thus dependent on both the emitted power and frequency of operation: the lower the frequency, the longer the range.

The maximum theoretical attenuation for ultrasonic energy can be approximated by (Shirley, 1989):

$$a_{\max} = \frac{f}{100}$$

where:
a_{max} = maximum attenuation in dB/foot
f = operating frequency in KHz.

For a 20-KHz transmission, a typical absorption factor in air is approximately 0.02 dB/foot, while at 40 KHz losses run between 0.06 and 0.09 dB/foot (Ma & Ma, 1984).

Combining the above spherical-divergence and molecular-absorption attenuation factors results in the following governing equation for intensity as a function of distance R from the source:

$$I = \frac{I_o\, e^{-2\alpha R}}{4\pi R^2}$$

Note that in this expression, which does not yet take into consideration any interaction with the target surface, intensity falls off with the square of the distance.

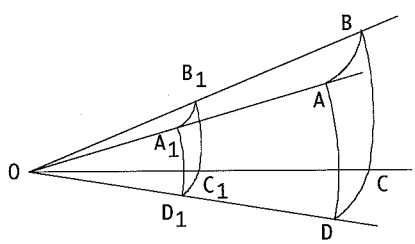

Figure 3: *Neglecting atmospheric attenuation, the total energy flowing within the cone OABCD is independent of the distance at which it is measured, whereas the intensity per unit area falls off with the square of R (adapted from Feynman, et al., 1963).*

Target Reflectivity. The totality of all energy incident upon a target object is either reflected or absorbed, be it acoustical, optical, or RF in nature. The directivity of the target surface determines how much of the reflected energy is directed back towards the transducer. Since most objects scatter the signal in an isotropic fashion, the returning echo again dissipates in accordance with the inverse square law (Biber, et al., 1980), introducing an additional $4\pi R^2$ term in the denominator of the previous equation for intensity. In addition, a new factor Kr must be introduced in the numerator to account for reflectivity of the target:

$$I = \frac{K_r\, I_o\, e^{-2\alpha R}}{16\pi^2 R^4}$$

where:
K_r = coefficient of reflection.

This coefficient of reflection for a planar wave arriving normal to a planar object surface is given by (Pallas-Areny & Webster, 1992):

$$K_r = \frac{I_r}{I_i} = \left(\frac{Z_a - Z_o}{Z_a + Z_o}\right)^2$$

where:
I_r = reflected intensity
I_i = incident intensity
Z_a = acoustic impedance for air
Z_o = acoustic impedance for the target object.

The bigger the impedance mismatch between the two media, the more energy will be reflected back to the source. In industrial applications, this phenomenon allows tank level measurement to be accomplished using an ultrasonic transducer in air looking down on the liquid surface, or alternatively an immersed transducer looking upward at the fluid/air interface.

Figure 4: *A small ball impacting a sawtooth surface as shown will generally bounce back towards its origin, whereas a ball much larger in diameter than the sawtooth dimension* d *will bounce away in specular fasion.*

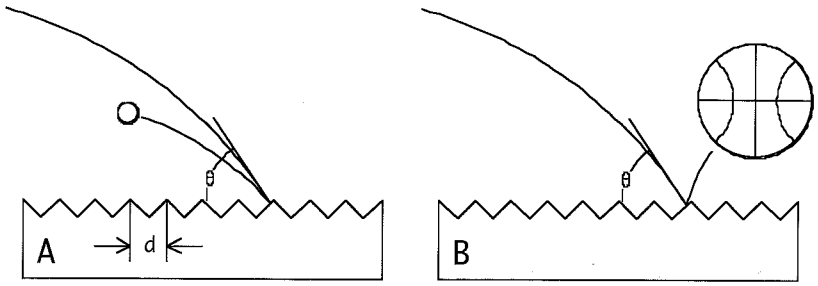

Most targets are specular in nature with respect to the relatively long wavelength (roughly 0.25 inch at 50 KHz) of ultrasonic energy, as opposed to being diffuse. In the case of specular reflection, the angle of reflection is equal to the angle of incidence, whereas for diffuse reflection energy is scattered in various directions by surface irregularities equal to or larger than the wavelength of incident radiation. Lambertian surfaces are ideal diffuse reflectors that in theory scatter energy with equal probability in all directions (Jarvis, 1983).

To develop a more or less intuitive appreciation for this relationship to wavelength, it is perhaps helpful to consider the analogy of a pair of rubber balls impacting a hypothetical surface with the sawtooth profile shown in Figure 4. Assume one ball is approximately an inch in diameter, while the other is a much larger basketball. If the sawtooth dimension *d* is in the same neighborhood as the diameter of the smaller ball, then there is a good chance this ball when approaching the surface at some angle of incidence θ will bounce back towards its origin as shown in Figure 4A. This is because on the scale of the smaller ball, the surface has a significant normal component. On the other hand, when the basketball impacts this sawtooth surface with the same angle of incidence, the surface irregularities are too small with respect to the ball diameter to be effective. The basketball therefore deflects in a specular manner as shown in Figure 4B.

A familiar example of this effect at optical wavelengths can be seen when the beam of an ordinary flashlight is pointed towards a wall mirror at roughly a 45-degree angle. The footprint of illumination on the mirror surface is not visible, because all the light energy is deflected away in a specular fashion. In other words, you can't see the flashlight spot on the mirror itself. Now suppose the flashlight is redirected slightly towards the wall adjacent to the mirror. The spot of light shows up clearly on the wall surface, which is Lambertian in nature with respect to the wavelength of light. The wall is thus a diffuse reflector as opposed to a specular reflector for optical energy.

When the angle of incidence of a sonar beam decreases below a certain critical value, the reflected energy does not return to strike the transducer. The obvious reason for this effect is the normal component falls off as the angle of incidence becomes more shallow, as illustrated in Figure 5.

Figure 5: *As the angle of incidence decreases below a certain critical angle, reflected energy no longer returns to the transducer.*

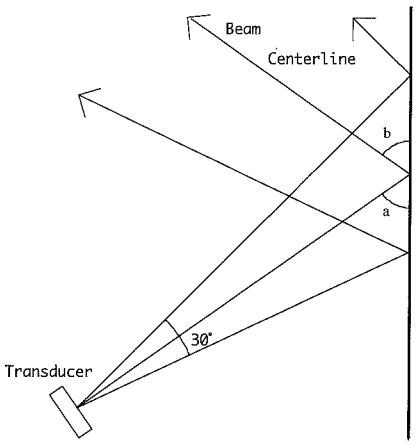

This critical angle is a function of the operating frequency chosen and the topographical characteristics of the target surface.

For the Polaroid electrostatic transducers this angle turns out to be approximately 65 degrees (i.e., 25 degrees off normal) for a flat target surface made up of unfinished plywood. Transducer offset from the normal will result in either a false echo as deflected energy returns to the detector over an elongated path, or no echo as the deflected beam dissipates. In Figure 5 above, the ranging system would not see the wall and indicate instead maximum range, whereas in Figure 6 the range reported would reflect the total round trip

Figure 6: *Due to specular reflection, the measured range would represent the round trip distance through points A, B, and C as opposed to the actual distance between A and B (adapted from Everett, 1985).*

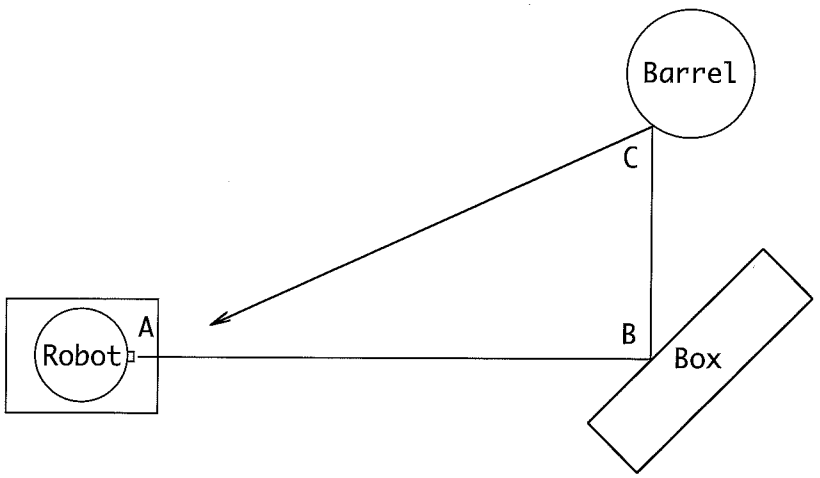

through points A, B, and C as opposed to just A and B.

When the first prototype of the Mobile Detection Assessment Response System (MDARS) interior robot (Figure 7) was delivered to another government laboratory for formal Technical Feasibility Testing in early 1991 (Holland, et al., 1995; Laird, et al., 1995), the narrow-beam collision avoidance sonar array experienced significant problems in the form of false echo detections. These erroneous sonar readings were quickly seen to correlate with the presence of expansion joints in the concrete floor surface of the test facility. The transducers in the forward-looking array were purposely installed with a 7-degree down angle to increase the probability of detection for low-lying obstructions. This approach had worked very well in our building over months of extended operations, because the smooth floors were very specular targets with no significant discontinuities. An overnight field change realigning the sonar beams to a horizontal orientation was required to resolve the problem (Everett, et al., 1994).

Any significant absorption can result in a reduction of the reflected wave intensity with an adverse impact on system performance. For example, the Polaroid ultrasonic system has an advertised range of 35 feet. In testing the security module on the MDARS robot, however, we found it was difficult to pick up an average size person standing upright much beyond a distance of 23 feet. Harder targets of smaller cross-sectional area, on the other hand, could be seen out to the maximum limit.

The amount of energy coupled into the target surface (i.e., absorbed) versus that reflected is basically determined by the difference in acoustic impedance Z between the propagation medium (air) and the target object itself. Typical values for Z are listed in Table 1. Maximum transmission of energy occurs in the case of a fully homogeneous medium where Z is uniform throughout. For non-homogeneous situations involving an interface between two dissimilar media, effective coupling falls off (and reflectivity subsequently goes up) as the differential in Z increases. The coefficient of transmission for a planar wave incident upon a planar target in a direction normal to the target surface is given by (Pallas-Areny & Webster, 1992):

$$K_t = \frac{I_t}{I_i} = \frac{4Z_a Z_o}{(Z_a + Z_o)^2}$$

where:

K_t = coefficient of transmission (absorption)
I_t = transmitted intensity
I_i = incident intensity
Z_a = acoustic impedance for air
Z_o = acoustic impedance for the target object.

The original Polaroid ranging module transmitted a 1-millisecond chirp consisting of four discrete frequencies: 8 cycles at 60 KHz, 8 cycles at 56 KHz, 16 cycles at 52.5 KHz, and 24 cycles at 49.41 KHz (Biber, et al., 1980). This technique was employed to increase the probability of signal reflection from the target, since certain surface characteristics could theoretically absorb a single-frequency waveform, preventing detection. In actual practice such frequency-dependent effects rarely arose, suggesting this aspect of the absorption problem

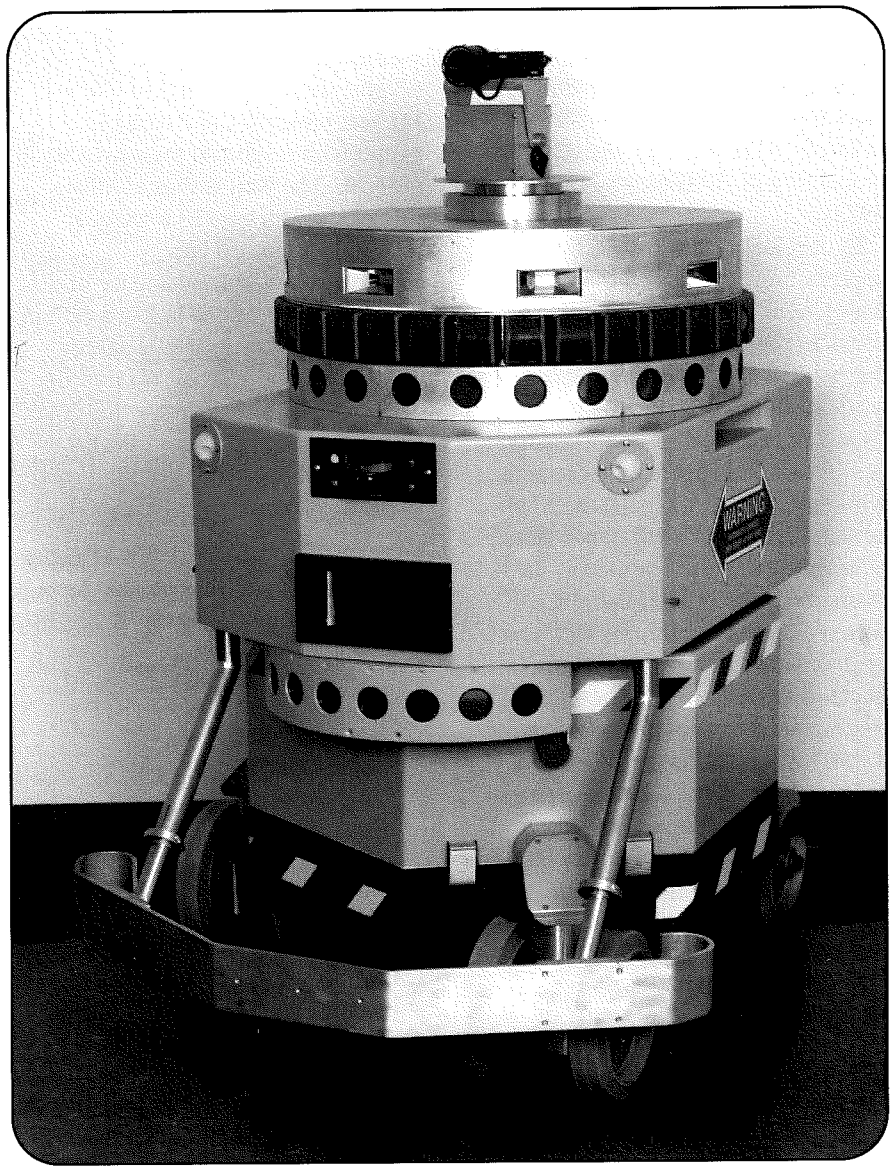

Figure 7: *The early feasibility prototype of the MDARS interior robot employed nine Polaroid electrostic sensors in a forward-looking collision avoidance array, as well as 24 additional sensors in a 360-degree array for ultrasonic motion detection (courtesy Naval Command Control and Ocean Surveillance Center).*

had been somewhat overestimated. In fact, Polaroid's improved version of the ranging module circuit board, the SN28827, operated at a single frequency of 49.1 KHz.

My daughter Rebecca compiled a significant amount of empirical data in 1993 as part of her high school science fair project entitled Determining the Accuracy of an Ultrasonic Ranging Sensor (Figure 8). One of her tests investigated the reflective properties of various target surfaces measuring 16 by 24 inches. The targets were maintained normal to a temperature-compensated Polaroid sensor (a Digitape ultrasonic tape measuring unit distributed by Houseworks) mounted 14 inches above a smooth concrete floor. Starting at a point beyond the maximum range of detection, the distance between the sensor and target was decreased in 1-foot increments until a valid range reading was obtained. The table (Table 2) is reproduced here with her permission.

Air Turbulence. Turbulence due to wind and temperature variations can cause bending or distortion of acoustical energy traveling through air (Shirley, 1989). Wind direction and velocity can have a noticeable push or delay effect on the wave propagation velocity, more relevant in the case of outdoor vehicles. Consideration of wind-effect errors must also treat crosswind components in addition to those which travel on a parallel path either with or against the wavefront. Crosswind effects can cause the beam center to be offset from its targeted direction, diminish the intensity of returned echoes, and result in a slightly longer beam path due to deflection.

In general, little effort is made in the case of mobile robotic applications to correct for such errors. This is probably due to the fact that ultrasonic ranging is most widely employed in indoor scenarios where the effects of air turbulence are minimal, unless extreme measurement accuracy is desired. In addition, there is really no practical way to reliably measure the phenomena responsible for the interference, and so compensation is generally limited to averaging over multiple readings. This approach introduces a coordinate transformation requirement in the case of a moving platform, since the slow speed of sound limits effective update rates to roughly 2 Hz (i.e., single transducer, assuming 28 feet maximum range). Faster updates are possible if the system is range-gated to some lesser distance (Gilbreath & Everett, 1988).

Table 1: *Typical values of acoustical impedance (Z) for various conducting media (adapted with permission from Bolz & Tuve, 1979, © CRC Press, Boca Raton, FL; and Pallas-Areny & Webster, 1992).*

Medium	Z	Units
Air	4.3×10^{-4}	million Pascal-seconds/meter
Cork	1.0	million Pascal-seconds/meter
Water	1.5	million Pascal-seconds/meter
Human tissue	1.6	million Pascal-seconds/meter
Rubber	3.0	million Pascal-seconds/meter
Glass	13	million Pascal-seconds/meter
Aluminum	17	million Pascal-seconds/meter
Steel	45	million Pascal-seconds/meter
Gold	62.5	million Pascal-seconds/meter

Temperature. Recall the earlier expression for wave propagation speed (s) in a gas, as a function of density ρ and bulk modulus of elasticity K_m:

$$s = \sqrt{\frac{K_m}{\rho}}$$

Since both of these parameters change with temperature, the speed of sound in air is also temperature dependent (Pallas-Areny & Webster, 1992), and in fact directly proportional to the square root of temperature in

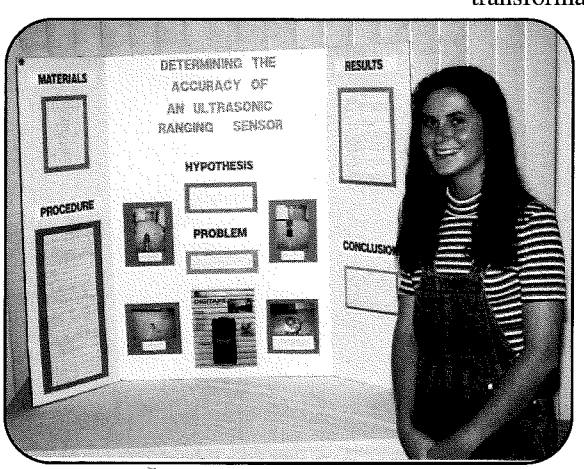

Figure 8: *Rebecca Everett checked the accuracy of the Polaroid sensor in measuring the distance to a variety of surfaces for her science project.*

Table 2: *Maximum detection ranges for standardized 16- by 24-inch cross-sections of various materials.*

Surface	Distance	Reading	Units
Plywood	24	24.2	feet
Towel	22	22.3	feet
Underside of rug	16	16.3	feet
Foam	13	13.3	feet
Pillow	9	9.4	feet
Blanket	8	8.4	feet
Top of rug	3	3.6	feet

degrees Rankine (Everett, 1985):

$$s = \sqrt{g\,k\,R\,T}$$

where:
s = speed of sound
g = gravitational constant
k = ratio of specific heats
R = gas constant
T = temperature in degrees Rankine (F + 460).

For temperature variations typically encountered in indoor robotic ranging applications, this dependence results in a significant effect even considering the short distances involved. A temperature change over the not unrealistic span of 60° to 90°F can produce a range error as large as 12 inches at a distance of 35 feet. Fortunately, this situation can be remedied through the use of a correction factor based upon the actual ambient temperature, available from an external sensor mounted on the robot. The formula is simply:

$$R_a = R_m \sqrt{\frac{T_a}{T_c}}$$

where:
R_a = actual range
R_m = measured range
T_a = actual temperature in degrees Rankine
T_c = calibration temperature in degrees Rankine.

The possibility does still exist, however, for temperature gradients between the sensor and the target to introduce range errors, since the correction factor is based on the actual temperature in the immediate vicinity of the sensor only. As in the case of air turbulence, there is generally little recourse other than averaging multiple readings. (Some industrial applications provide a temperature-stabilized column of air using a small blower or fan.)

Beam Geometry. Still another factor to consider is the beamwidth of the selected transducer, defined as the angle between the points at which the sound power has been reduced to half (-3 dB) its peak value (Shirley, 1989). This formal definition does not always map directly into any useful parameter in real-world usage, however. What is generally of more concern can be better described as the effective beamwidth, or the beam geometry constraints within which objects are reliably detected. (Reliable detection, of course, is also very much dependent on the size and shape of the object.) The width of the beam is determined by the transducer diameter and the operating frequency. The higher the frequency of the emitted energy, the narrower and more directional the beam, and hence the greater the angular resolution. Recall, however, an increase in frequency causes a corresponding increase in signal attenuation in air and decreases the maximum range of the system.

The wavelength of acoustical energy is inversely proportional to frequency as shown below:

$$\lambda = \frac{s}{f}$$

where:
λ = wavelength
s = speed of sound
f = operating frequency.

The beam-dispersion angle is directly proportional to this transmission wavelength (Brown, 1985):

$$\theta = 1.22\frac{\lambda}{d}$$

where:
θ = desired dispersion angle
λ = acoustic wavelength
d = transducer diameter.

The above relationship can be intuitively visualized by considering the limiting case where d approaches zero. Such a hypothetical device would theoretically function as a point source, emitting energy of equal magnitude in all directions. As d is increased, the device can be considered a planar array of point sources clustered together in circular fashion. For this configuration, the emitted energy will be in phase and at maximum intensity only along a surface normal. Destructive interference from adjacent point sources causes the beam intensity to fall off rapidly to either side, up to some local minimum value as shown in Figure 9. Constructive interference then occurs past this minimum point, resulting in the presence of side lobes.

Shirley (1989) defines the spot diameter that is insonified by the ultrasonic beam (*i.e.*, footprint of the incident beam at the target surface) in terms of this beam-dispersion angle θ (Figure 10):

$$D = 2\,R\,\tan\frac{\theta}{2}$$

where:
D = spot diameter
R = target range.

Best results are obtained when the beam centerline is maintained normal to the target surface. As the angle of incidence varies from the perpendicular, note the range actually being measured does not always correspond to that associated with the beam centerline (Figure 11). The beam is

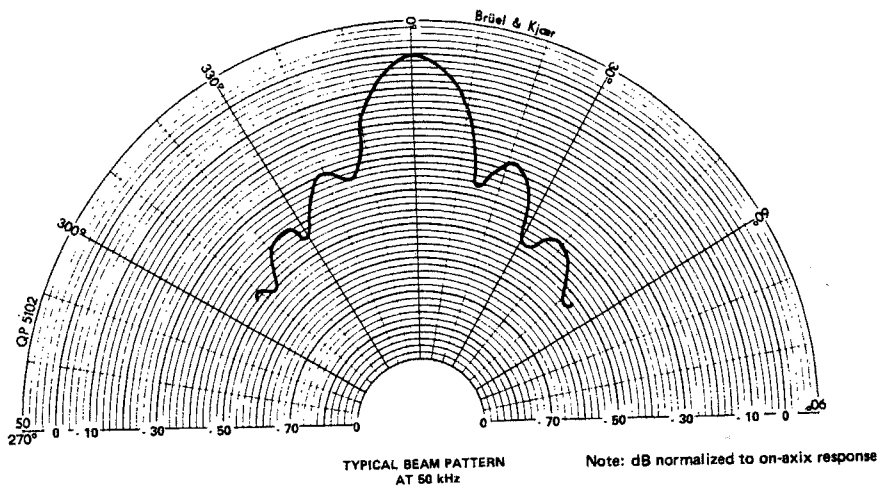

Figure 9: *Constructive interference results in maximum power in the main lobe along the beam center axis (courtesy of Polaroid Corp.).*

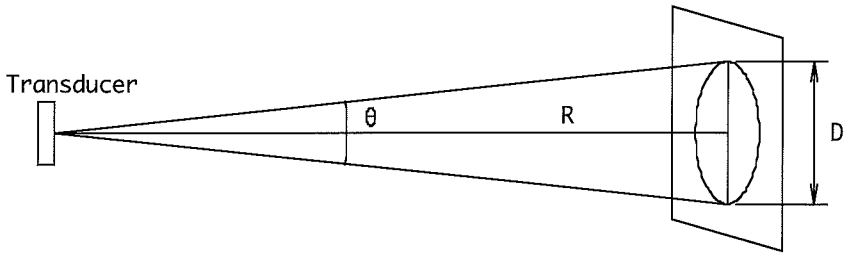

Figure 10: *The diameter of the insonified footprint at the target surface, assuming normal incidence.*

reflected first from the portion of the target closest to the sensor. For a 30-degree beam-dispersion angle at a distance of 15 feet from a flat target, with an angle of incidence of 70 degrees with respect to normal, the theoretical error could be as much as 10 inches. The actual line of measurement intersects the target surface at point B as opposed to point A.

Effective beamwidth introduces some uncertainty in the perceived distance to an object from the sensor but an even greater uncertainty in the angular resolution of the object's position. A very narrow target, such as a vertical pole, would have a relatively large associated region of floor space that would essentially appear to the sensor to be obstructed. Worse yet, a 3-foot doorway may not be discernible at all when only 6 feet away, simply because at that distance the beam is wider than the door opening.

Improved angular resolution can sometimes be obtained through beam splitting, a technique that involves the use of two or more transducers with partially overlapping beam patterns. Figure 12 shows how for the simplest case of two transducers, twice the angular resolution can be obtained along with a 50-percent increase in coverage area. If the target is detected by both sensors A and B, then it (or at least a portion of it) must lie in the region of overlap shown by the shaded area. If detected by A but not B, then it lies in the region at the top of the figure, and so on. Increasing the number of sensors with overlapping beam patterns decreases the size of the respective regions, and thus increases the angular resolution.

It should be noted, however, that this increase in angular resolution is limited to the case of a discrete target in relatively uncluttered surroundings, such as a metal pole supporting an overhead load or a lone box in the middle of the floor. No improvement is seen for the case of an opening smaller than an individual beamwidth, such as a doorway. The entire beam from at least one sensor must pass through the opening without striking either side in order for the opening to be detected, and the only way to improve resolution otherwise is to decrease the individual beamwidths by increasing the operating frequency, changing transducers, or through acoustical focusing. Some designs achieve this effect through use of an attachable horn that concentrates the energy into a tighter, more powerful beam (Shirley, 1989).

A number of factors must be considered when choosing the optimal beamwidth for a particular application. A narrow beamwidth will not detect unwanted objects to either side, is less susceptible to background noise, and can achieve greater ranges since the energy is more concentrated (Shirley, 1989). On the other hand, for collision avoidance applications it is often desirable to detect any and all objects in front of the robot, and since extremely long ranges are not usually required, a wide-angle transducer may be a more optimal choice (Hammond, 1993). When comparing a single transducer of each type, the use of a wide beamwidth will improve chances of target detection due to the greater likelihood of some portion of the beam encountering a surface normal condition as seen in Figure 13. Admittedly this observation is a bit like saying the wider the beam, the more chance of hitting a target. Taken to the extreme, a hypothetical 360-degree field-of-view transducer is clearly of rather limited utility due to the total lack of azimuthal information regarding the target's whereabouts.

Alternatively, an equivalent surface-normal condition can be realized using a cylindrical array of narrow-

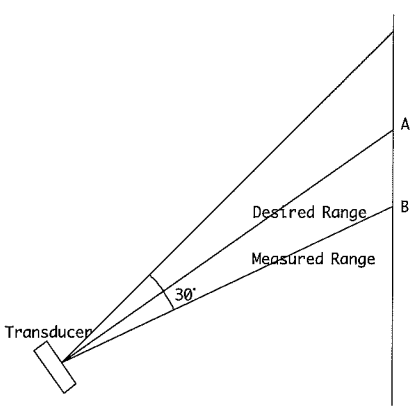

Figure 11: *Ultrasonic ranging error due to beam divergence results in a shorter range measurement to the target surface at B instead of the desired reading to point A.*

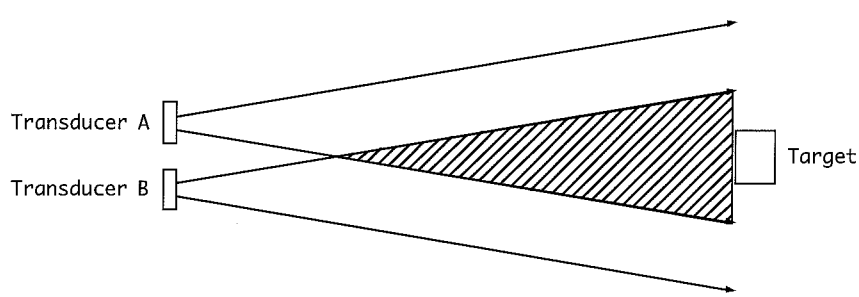

Figure 12: *Beam-splitting techniques using two or more sensors can improve angular resolution for discrete targets (adapted from Everett, 1985).*

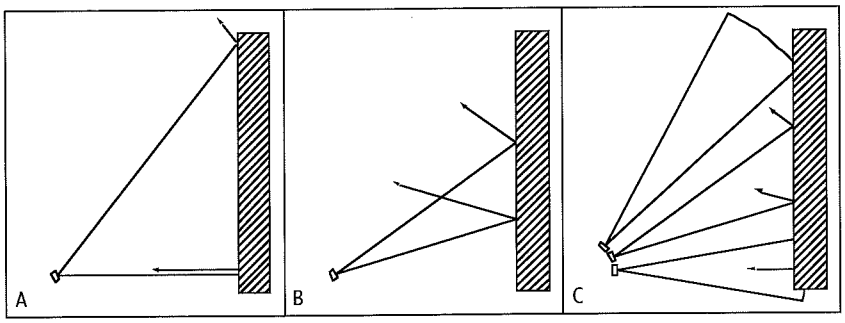

Figure 13: *A wide-angle transducer (A) has a greater chance of encountering a surface normal condition than a single narrow-beam transducer (B), but at the expense of reduced angular resolution and effective range. A more optimal configuration is presented in (C), at a slight cost to system update rate.*

beam transducers to achieve the same volumetric coverage as illustrated in Figure 13C. This approach offers the added advantage of significantly improved angular resolution but at the expense of a slower overall update rate. The MDARS Interior robot uses a combination of wide-angle piezoelectric sonars operating at a frequency of 75 KHz for timely obstacle detection coverage, and a nine-element array of narrow-beam Polaroid electrostatic transducers operating at 49.4 KHz to support intelligent obstacle avoidance. Detection of any potential obstructions by either type of sonar causes the platform to slow to a speed commensurate with the narrow-beam update rate, whereupon the high-resolution Polaroid data is used to formulate an appropriate avoidance maneuver.

Noise. Borenstein & Koren (1992) of the University of Michigan Mobile Robotics Lab define three types of noise affecting the performance of ultrasonic sensors:

- *Environmental noise* resulting from the presence of external sources operating in the same space. Typical examples in industrial settings include high-pressure air blasts and harmonics from electrical arc welders.
- *Crosstalk* resulting from the proximity of other sensors in the group, which can be especially troublesome when operating in confined areas.
- *Self noise* generated by the sensor itself.

A noise-rejection measure for each of the components was developed and integrated into a single algorithm (Michigan, 1991), which was in turn combined with a fast sensor-firing algorithm. This software has been implemented and tested on a mobile platform that was able to traverse an obstacle course of densely packed 8-millimeter-diameter poles at a maximum velocity of 1 meter/second.

System-Specific Anomalies. A final source of error to be considered stems from case-specific peculiarities associated with the actual hardware employed. We shall again refer to the Polaroid system, in light of its widespread usage, as an illustrative example in the ensuing discussion.

Pulse Width. The 1-millisecond length of the original four-frequency Polaroid chirp was a potential source of range measurement error since sound travels roughly 1100 feet/second at sea level, which equates to about 13 inches/millisecond. The uncertainty and hence error arose from not knowing which of the four frequencies making up the chirp actually returned to trigger the receiver, but timing the echo always began at the start of the chirp (Everett, 1985). For the initial application of automatic camera focusing, designers were less concerned about absolute accuracy than missing a target altogether due to surface absorption of the acoustical energy. The depth-of-field of the camera optics would compensate for any small range errors that might be introduced due to this chirp ambiguity.

Even with the more recent SN28827 ranging model operating at a single frequency of 49.1 KHz, the transmission pulse duration is 0.326 milliseconds, giving rise to a maximum theoretical error of approximately 1.7 inches. (This estimate takes into account round-trip distance, and assumes best-case echo detection after just three cycles of returned energy.) The new Polaroid Ultrasonic Ranging Developer's Kit allows for programmable pulse duration to alleviate this limitation in demanding applications (Polaroid, 1993).

Threshold Detection. The specific method for detection of the returned pulse can be a significant source of error in any TOF ranging system (Figueroa & Lamancusa, 1992). Kuc and Siegel (1987) point out that the intensity of a typical pulse transmission peaks in the second cycle (Figure 14), and so simple thresholding of the received signal can cause late detection of weak echoes. Leonard and Durrant-Whyte (1992) discuss further complications in the

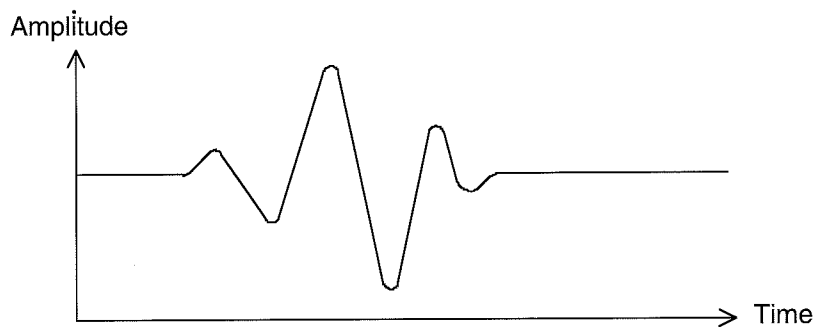

Figure 14: *A typical pulse waveform for an electrostatic transducer can be approximated by a sinusoid that is modulated by a Gaussian envelope, peaking in intensity during the second cycle (Kuc & Siegel, 1987, © IEEE).*

specific case of the integrating capacitive threshold detector employed in the Polaroid ranging module. This integrative approach was incorporated by the designers to discriminate against unwanted noise spikes (Biber, et al., 1980). Compared to strong reflections, valid but weak echo returns can take substantially longer to charge up the capacitor to the threshold level required for the comparator to change state.

The effect of this charging delay is to make those targets associated with weaker returns appear further away. Ignoring the obvious worst-case scenario of a completely missed echo, maximum theoretical error is bounded by the length of the transmitted burst. The obvious question now becomes, which is more preferable: missing target detection altogether, or being alerted to target presence at the expense of range accuracy? The answer of course depends on the particular priorities of the application addressed. If the ranging sensor is being employed as a presence detector for security purposes, precise accuracy is not all that important. On the other hand, if the sensor is being used for navigational referencing, the situation may be somewhat different.

Stepped Gain. Lang, et al. (1989) experimentally confirmed error effects associated with the piecewise 16-step gain ramp employed on the earlier Polaroid 607089 ranging module. In order to precisely counter the effects of signal loss as a function of range-to-target (*i.e.*, due to atmospheric attenuation and spherical divergence), the actual time-dependent gain compensation would be an exponential function inversely related to the spherical divergence equation presented earlier (see the Atmospheric Attenuation section). A rather coarse piecewise approximation to this ideal gain curve (Figure 15) naturally results in a situation where the instantaneous amplifier gain is: 1) correct only for a single point in time over the period represented by a specific step value, 2) excessive prior to this point, and 3) insufficient afterwards. If the gain is too low at the time of reflected pulse train arrival, weak echoes are either missed entirely or delayed in triggering the integrating detector, resulting in an erroneous increase in the perceived range.

Choosing an Operating Frequency. The operating frequency of an ultrasonic ranging system should be selected only after careful consideration of a number of factors, such as the diameter and type of transducer, anticipated target characteristics, sources of possible interference, and most importantly the nature of the intended task, to include desired angular and range resolution. Resolution is dependent on the bandwidth of the transmitted energy, and greater bandwidth can be achieved at higher frequencies but at the expense of maximum effective range. The minimum ranging distance is also a function of bandwidth, and thus higher frequencies are required in close as the distance between the detector and target decreases. Most man-made background noise sources have energy peaks below 50 KHz (Hammond, 1993), however, and so higher-frequency systems are generally preferred in acoustically noisy environments (Shirley, 1989).

About the Author

Commander H. R. (Bart) Everett, USN (Ret.), is the former Director of the Office of Robotics and Autonomous Systems at the Naval Sea Systems Command, Washington, DC. He currently serves as Technical Director for the tri-service Mobile Detection Assessment Response System (MDARS) robotic security program under development at the Naval Command Control and Ocean Surveillance Center, San Diego, CA.

Active in the field of robotics research for over 20 years, with personal involvement in the development of 11 mobile systems, he has published over 70 technical papers and reports and has 16 related patents issued or pending. He serves on the Editorial Board for *Robotics and Autonomous Systems* magazine and on the Board of Directors for the International Service Robot Association, and is a member of Sigma Xi, the Institute of Electrical and Electronics Engineers (IEEE), and the Association for Unmanned Vehicle Systems (AUVS).

References

Asher, R.C., "Ultrasonic Sensors in the Chemical and Process Industries," Journal of Physics E.: Scientific Instruments, Vol. 16, pp. 959-963, 1983.

Bartram, J.F., Ehrlich, S.L., Fredenberg, D.A., Heimann, J.H., Kuzneski, J.A., Skitzki, P., "Underwater Sound Systems," in *Electronic Engineer's Handbook*, D. Christiansen and D. Fink, eds., 3rd edition, McGraw Hill, New York, NY, pp. 25.95-25.133, 1989.

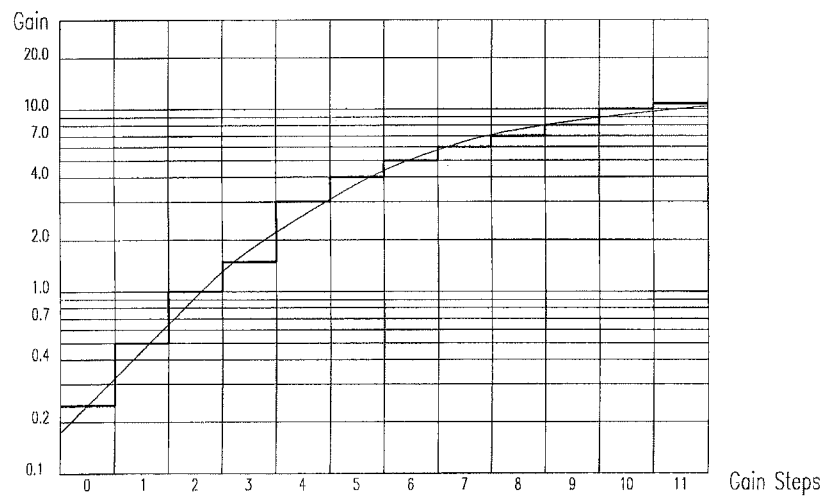

Figure 15: *The 12-step approximation employed in the new 6500-series receiver gain ramp results in a situation where the instantaneous gain is either above or below the ideal value for most of the step duration (adapted from Polaroid, 1993). Note the large jump in gain between steps 3 and 4.*

Biber, C., Ellin, S., Shenk, E., "The Polaroid Ultrasonic Ranging System," Audio Engineering Society, 67th Convention, New York, NY, October-November, 1980.
Bolz, R.E., Tuve, G.L., *CRC Handbook of Tables for Applied Engineering Science*, CRC Press, Boca Raton, FL, 1979.
Borenstein, J, Koren, Y., "Error Eliminating Rapid Ultrasonic Firing for Mobile Robot Obstacle Avoidance," IEEE International Conference on Robotics and Automation, Nice, France, May, 1992.
Brown, M.K., "Locating Object Surfaces with an Ultrasonic Range Sensor," IEEE Conference on Robotics and Automation, St. Louis, MO, pp.110-115, March, 1985.
Campbell, D., "Ultrasonic Noncontact Dimensional Measurement," *Sensors*, pp. 37-43, July, 1986.
Dunkin, W.M., "Ultrasonic Position Reference Systems for an Autonomous Sentry Robot and a Robot Manipulator Arm", Masters Thesis, Naval Postgraduate School, Monterey, CA, March, 1985.
Everett, H.R., "A Multielement Ultrasonic Ranging Array," *Robotics Age*, pp.13-20 July, 1985.
Everett, H.R., Gage, D.W., Gilbreath, G.A., Laird, R.T., Smurlo, R.P., "Real-world Issues in Warehouse Navigation," SPIE Mobile Robots IX, Vol. 2352, Boston, MA, November, 1994.
Feynman, R.P., Leighton, R.B., Sands, M., *The Feynman Lectures on Physics*, Vol. 1, Addison-Wesley, Reading, MA, 1963.
Figueroa, F., Barbieri, E., "Increased Measurement Range Via Frequency Division in Ultrasonic Phase Detection Methods," *Acustica*, Vol. 73, pp. 47-49, 1991.
Figueroa, J.F., Lamancusa, J.S., "A Method for Accurate Detection of Time of Arrival: Analysis and Design of an Ultrasonic Ranging System," Journal of the Acoustical Society of America, Vol. 91, No. 1, pp. 486-494, January, 1992.
Figueroa, J.F., Mahajan, A., "A Robust Navigation System for Autonomous Vehicles Using Ultrasonics," *Control Engineering Practice*, Vol. 2, No. 1, pp. 49-59, 1994.
Fox, J.D., Khuri-Yakub, B.T., Kino, G.S., "High-Frequency Acoustic Wave Measurements in Air," IEEE Ultrasonics Symposium, pp. 581-584, 1983.
Frederiksen, T.M., Howard, W.M., "A Single-Chip Monolithic Sonar System," *IEEE Journal of Solid State Circuits*, Vol. SC-9, No. 6, December, 1974.
Gilbreath, G.A., Everett, H.R., "Path Planning and Collision Avoidance for an Indoor Security Robot," SPIE Mobile Robots III, Cambridge, MA, pp. 19-27, Novemeber, 1988.
Halliday, D., Resnick, R., *Fundamentals of Physics*, John Wiley, New York, NY, 1974.
Hammond, W., "Smart Collision Avoidance Sonar Surpasses Conventional Systems," *Industrial Vehicle Technology '93: Annual Review of Industrial Vehicle Design and Engineering*, UK and International Press, pp. 64-66, 1993.
Holland, J.M., Martin, A., Smurlo, R.P., Everett, H.R., "MDARS Interior Platform," Association of Unmanned Vehicle Systems, 22nd Annual Technical Symposium and Exhibition (AUVS '95), Washington, DC, July, 1995.
Irwin, C.T., Caughman, D.O., "Intelligent Robotic Integrated Ultrasonic System," Proceedings, Robots 9, Society of Manufacturing Engineers, Detroit, MI, Sect. 19, pp. 38-47, June, 1985.
Jarvis, R.A., "A Laser Time-of-Flight Range Scanner for Robotic Vision," *IEEE Transactions on Pattern Analysis and Machine Intelligence*, Vol. PAMI-5, No. 5, pp. 505-512, 1983.
Kuc, R., Siegel, M.W., "Physically Based Simulation Model for Acoustic Sensor Robot Navigation," IEEE Transactions on Pattern Analysis and Machine Intelligence, Vol. PAMI-9, No. 6, pp. 766-778, November, 1987.
Laird, R.T., Gilbreath, G.A., Heath-Pastore, T.A., Everett, H.R., Inderieden, R.S., Grant, K., "MDARS Multiple Robot Host Architecture," Association of Unmanned Vehicle Systems, 22nd Annual Technical Symposium and Exhibition (AUVS '95), Washington, DC, July, 1995.
Lang, S., Korba, L., Wong, A., "Characterizing and Modeling a Sonar Ring," SPIE Mobile Robots IV, Philadelphia, PA, pp. 291-304, 1989.
Leonard, J.J., Durrant-Whyte, H.F., *Directed Sonar Sensing for Mobile Robot Navigation*, Kluwer Academic Publishers, Boston, MA, 1992.
Ma, Y.L., Ma, C., "An Ultrasonic Scanner System Used on an Intelligent Robot," IEEE IECON '84, Tokyo, Japan, pp. 745-748, October, 1984.
Michigan, "Mobile Robotics Lab," Brochure, University of Michigan Mobile Robotics Lab, Ann Arbor, MI, 1991.
Milner, R., ""Measuring Speed and Distance with Doppler," *Sensors*, pp. 42-44, October, 1990.
Mitome, H., Koda, T., Shibata, S., "Double Doppler Ranging System Using FM Ultrasound," *Ultrasonics*, pp. 199-204, September, 1984.
Pallas-Areny, R., Webster, J.G., "Ultrasonic Based Sensors," *Sensors*, pp. 16-20, June, 1992.
Polaroid, "Polaroid Ultrasonic Ranging Developer's Kit," Publication No. PXW6431 6/93, Polaroid Corporation, Cambridge, MA, June, 1993.
Shirley, P.A., "An Introduction to Ultrasonic Sensing," *Sensors*, pp. 10-17, November, 1989.
Shirley, P.A., "An Ultrasonic Echo-Ranging Sensor for Board Inspection and Selection," *Sensors*, June, 1991.
Smurlo, R.P., Everett, H.R., "Intelligent Sensor Fusion for a Mobile Security Robot," *Sensors*, pp. 18-28, June, 1993.
Ulrich, R., *Principles of Underwater Sound for Engineers*, 1983.